Instrument effects in polarized infrared images

Joseph A. Shaw, MEMBER SPIE
NOAA Environmental Technology Laboratory
325 Broadway
Boulder, Colorado 80303
and
University of Arizona
Optical Sciences Center
Tucson, Arizona 85721
E-mail: jshaw@etl.noaa.gov

Michael R. Descour, MEMBER SPIE
University of Arizona
Optical Sciences Center
Tucson, Arizona 85721

Abstract. We describe three instrument effects that cause polarized infrared images of a blackbody source to exhibit intriguing polarization dependence and image nonuniformity. The origins of these problems are reflection of background radiation from the wire-grid polarizer and frictional heating of the polarizer mount. Our model shows that the two surfaces of a wire-grid polarizer act like a partial polarizer-analyzer pair for reflected radiance. These effects must be considered carefully in applications such as polarimetric remote sensing, which require calibration uncertainties less than 1%.

Subject terms: infrared polarization; thermal imaging; remote sensing.

Optical Engineering 34(5), 1396--1399 (May 1995).

1 Introduction

Polarization in some cases contains useful information that can be exploited in infrared imaging. Some recent applications of infrared polarization imagery include astronomy' and detection of man-made objects.[2,3] We are investigating various polarization imaging techniques for environmental remote sensing. For example, it may be possible to use polarized infrared imagery to infer ocean wave-tilt spectra passively, in a fashion analogous to the visible polarization imaging of Churnside et al.[4] Recent calculations[5] suggest that it also may be useful to study cirrus clouds with polarized infrared imaging. Because such applications require measurement uncertainties on the order of 1 %, instrument polarization effects are critical.

In our initial experiments, we used a 3- to 5- μ m camera with a 256-by-320-pixel InSb detector array to view an extended-area, near-ambient blackbody source through a wire-grid polarizer. The image was quite nonuniform, and when we rotated the polarizer we observed two surprising effects: (1) a signal oscillation having periodic components at 180 and 360 deg, and (2) a net signal increase following a polarizer rotation, In this paper we demonstrate that the image nonuniformity and the 180-deg periodic polarization oscillation can be explained by reflection of ambient radiation into the camera by the wire-grid polarizer, and the signal rise is due to frictional heating (3.5 K) of the polarizer mount as it is rotated.

Paper 33084 received Aug. 31, 1994; revised manuscript received Dec. 17. 1994; accepted for publication Dec. 18, 1994.
 0091-3286/95/$6.00.

2 Image Nonuniformity Due to Narcissus

Figure 1 shows the mean camera output for two lo-pixel square regions in an image of an extended-area blackbody source, plotted versus polarizer angle. In the first region (a) a variation of about 1% of the mean output occurs with a 180-deg period (a smaller component with a 360-deg period is evident also), while in the second region (b) no systematic variation is evident. For now, however, we concentrate on the mean levels of the two image regions, which differ by about 9%.

The polarizer was close to the camera to fill its field of view when we recorded the data in Fig. 1. On moving the camera back to image the polarizer, we saw the narcissus[6] spot shown in Fig. 2. In this image the polarizer mount, the bright blackbody source behind the mount, and the round 50-mm-diam polarizer are evident. The narcissus spot is the black (cold) circle near the top of the polarizer in this image. Narcissus occurs because all detector pixels that view the blackbody see essentially the same source emission, but they see different radiances reflected from the polarizer substrate: on-axis pixels see cold detector radiance, while off-axis pixels see warm ambient radiance. Tilting the polarizer causes the narcissus spot to wander within, or even out of, the image.

As a consequence of the polarizer being close to the camera for Fig. 1, the image of the blackbody appeared quite nonuniform, because superposed on it was an out-of-focus narcissus spot. The darkest regions of the blurred image are on-axis pixels, while the brighter regions of the image are off-axis pixels. Hence, the mean signal for the off-axis region of Fig. l(a) is approximately 9% higher (warmer) than that of the on-axis region of Fig. l(b).

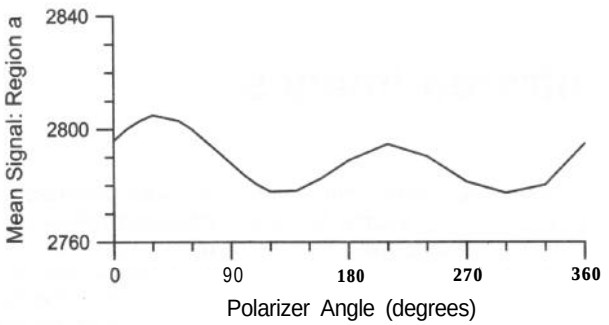

(a)

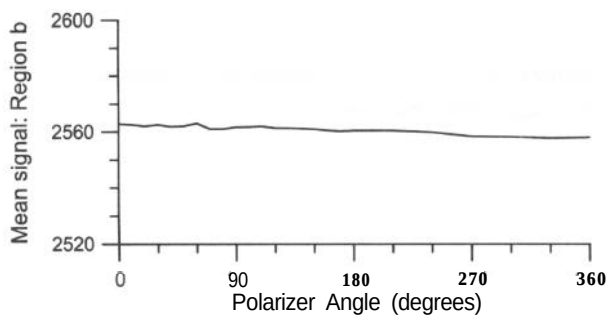

(b)

Fig. 1 Mean camera signal for two regions in an image of an unpolarized blackbody source. Region a is off axis, while region b is on axis.

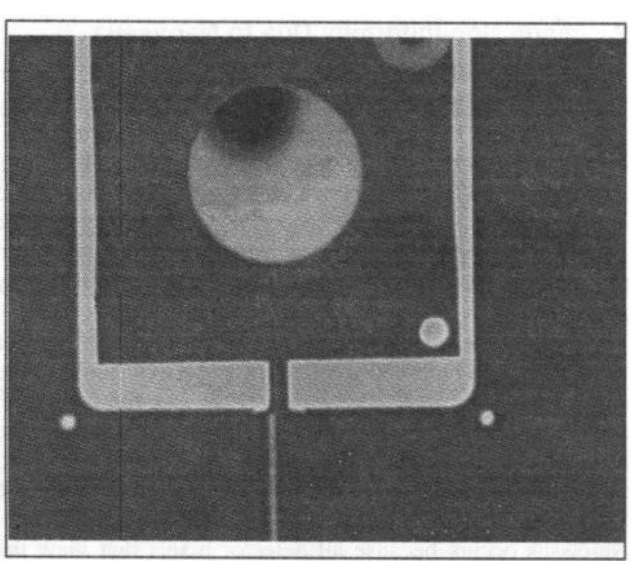

Fig. 2 Infrared image of the polarizer in front of the blackbody source. The dark spot near the top of the polarizer is caused by narcissus.

3 Partially Polarized Reflected Radiance

Variations in reflected radiation from a single surface can produce the small 360-deg component evident in Fig. l(a) as the polarizer is rotated around an axis that is not aligned perfectly with the principal optical axis. However, a single-surface reflection cannot cause the 180-deg component of the variation, even though the detected light is partially polarized, because the detector, has no polarization sensitivity.

The source of the 180-deg-periodic variation is the polarizer, whose two surfaces form what amounts to a polarizer-analyzer pair. Referring to the polarizer geometry shown in Fig. 3, the plain ZnSe surface behaves as a circularly symmetric partial analyzer, while the wire-grid surface behaves as an asymmetric polarizer. Rotating the actual polarizer can be thought of as rotating the asymmetric polarizer with respect to the fixed analyzer. Without the relative rotational asymmetry of these two surfaces, the detected radiance would be highly polarized, but would have no 180-deg component of variation.

At the air-ZnSe interface, ambient radiance reflects (R) and transmits (T) according to the Fresnel equations,[7]

$$R_p^{zs} = \frac{\tan^2(\theta_i - \theta_t)}{\tan^2(\theta_i + \theta_t)}, \tag{1a}$$

$$R_s^{zs} = \frac{\sin^2(\theta_i - \theta_t)}{\sin^2(\theta_i + \theta_t)}, \tag{1b}$$

$$T_p^{zs} = \frac{\sin(2\theta_i)\,\sin(2\theta_t)}{\sin^2(\theta_i + \theta_t)\,\cos^2(\theta_i - \theta_t)}, \tag{1c}$$

$$T_s^{zs} = \frac{\sin(2\theta_i)\,\sin(2\theta_t)}{\sin^2(\theta_i + \theta_t)}. \tag{1d}$$

In Eqs. (1a)–(1d), θ_i is the angle of incidence at the ZnSe surface, θ_t is the angle of the ray transmitted into the ZnSe, the superscript zs indicates a coefficient for the first ZnSe surface, and the subscripts *p* and *s* indicate the components parallel and perpendicular, respectively, to the plane of incidence defined by the incident ray and the surface normal.

The partially polarized transmitted radiance reflects from the second interface with even stronger polarization dependence because of the wire grid on the ZnSe substrate. A perfect wire grid passes the radiance polarized perpendicular to the grid and completely reflects the radiance polarized parallel to the grid. Therefore, for a horizontal polarizer grid, the reflectivities are $R_p^h = 1$ for p-polarized radiance and

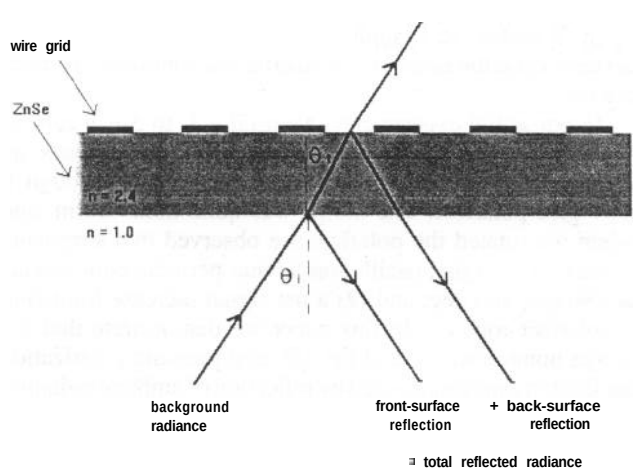

Fig. 3 The polarizer, consisting of a wire grid etched onto a ZnSe substrate. For both *p*- and *s-polarized* incident radiance, there are two reflected components: one from the air-ZnSe interface, and one from the ZnSe-grid interface.

R_s^h = (ZnSe-air reflectivity) for s-polarized radiance. For a vertical grid, the reflectivities are R_p^v = (ZnSe-air reflectivity) for p-polarized radiance and $R_s^v = 1$ for s-polarized radiance (the superscripts *h* and v indicate a horizontal or vertical polarizer grid, and the subscripts ***p*** and ***s*** indicate the radiance polarization state).

The radiance reflected by the second interface is partially transmitted back through the first interface according to Eqs. (lc) and (1d). Combining terms, the total reflectivities for *p* and ***s*** polarization are

$$R_p^{tot} = R_s^{zs} + (T_s^{zs})^2 R_p^x \tag{2a}$$

and

$$R_s^{tot} = R_s^{zs} + (T_s^{zs})^2 R_s^x , \tag{2b}$$

where $L^x_{p,s}$ is the wire-grid reflectivity discussed above, and the superscript ***x*** represents either *h* or *v*, determined by the polarizer grid orientation.

To estimate the relative polarization variation in the detected signal we evaluated the **Planck** function for spectral radiance, $L(l, T_s)$, at the center-band wavelength (λ = 4 μ m) for the emitted and reflected components. We used an ambient temperature of 300 K, a variable source temperature T_s, zero emissivity for the low-absorption **ZnSe** polarizer, and unity emissivity for the blackbody source and the ambient background. The resulting polarization-dependent radiances seen by the camera for a vertically oriented polarizer grid are approximately

$$L_p = (T_p^{zs})^2 L(4\ \mu\text{m}, T_s) + (R_p^{tot}) L(4\ \mu\text{m}, 300\ \text{K}) \tag{3a}$$

and

$$L_s = (R_s^{tot}) L(4\ \mu\text{m}, 300\ \text{K}) , \tag{3b}$$

while for a horizontal polarizer grid the radiances are

$$L_p = (R_p^{tot}) L(4\ \mu\text{m}, 300\ \text{K}) \tag{4a}$$

and

$$L_s = (T_s^{zs})^2 L(4\ \mu\text{m}, T_s) + (R_s^{tot}) L(4\ \mu\text{m}, 300\ \text{K}) . \tag{4b}$$

The quantity of interest is the percentage change in radiance seen by an off-axis pixel for horizontal and vertical polarizer grids,

$$\Delta L(\theta) = 100 \frac{(L_p^h + L_s^h) - (L_p^v + L_s^v)}{L_{ave}} . \tag{5}$$

In Eq. (5) the superscripts *h* and v indicate the grid orientation (horizontal or vertical), the subscripts *p* and ***s*** indicate *p*- or s-polarized incident radiance, and L_{ave} is the average of the total radiances with the grid oriented horizontally and vertically.

The percentage radiance change (Δ L) is shown in Fig. 4 for a variety of source temperatures and a 300-K ambient temperature. The curves for T_s = 190 and 270 K define the error range relevant to cloud measurements. The T_s = 310-K curve is close to what we expect for ocean-wave imaging. The error is larger for lower source temperatures, for which the reflected warm background radiance is more dominant.

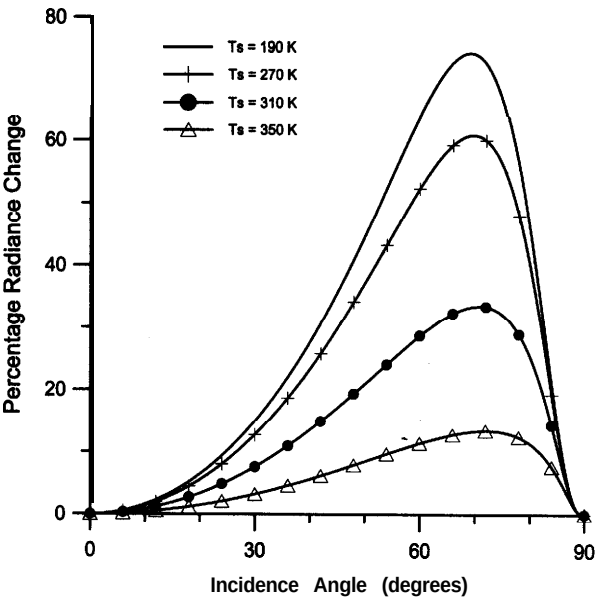

Fig. 4 Percentage change in radiance seen by a detector pixel as the polarizer rotates from horizontal to vertical. Each curve is for the labeled source temperature and a 300-K background temperature.

In Fig. 4, the curve for T_s = 310 K is appropriate for our laboratory measurements. The data shown in Fig. l(a) are for a pixel region (hence incidence angle) near 10 deg, for which our model predicts a polarization variation of about 1%. In fact, the measurements do show this magnitude of variation. Similarly, the on-axis image region of Fig. l(b) has no noticeable systematic polarization variation, as predicted. Angles larger than this see rapidly increasing AL. For example, a pixel at 20 deg will see a polarization variation of about **5%**, which is probably an unacceptable error in any polarization imaging application.

4 Frictional Polarizer-Mount Heating

Figure **5** demonstrates the other undesirable effect, a signal that increased as we rotated the polarizer (these data are from an on-axis pixel, to suppress the previously discussed polarization variation). When we left the polarizer in one position following a rotation, the signal returned slowly to its initial value.

We taped pieces of insulating foam on the polarizer mount to see if the problem was actually caused by transfer of body heat to the mount, but the change was small. What did make a large difference was turning on the equipment and letting it stabilize together for an hour before starting the experiment. Without this equalization period, the signal increased 30% during the rotation cycle; with it, the increase was only 3%. Apparently the blackbody source heats up the polarizer mount, it radiates into the polarizer, and the polarizer reflects some of this radiance into the camera. Note, however, that even when allowed to reach equilibrium with its surroundings, the polarizer mount tends to heat up several degrees during rotation.

A simple model is to calculate the percentage signal change as

$$\delta\,\text{sig} = 100 \frac{[L(T_{hi}) - L(T_{lo})] R_{ave}}{L_{ave}} , \tag{6}$$

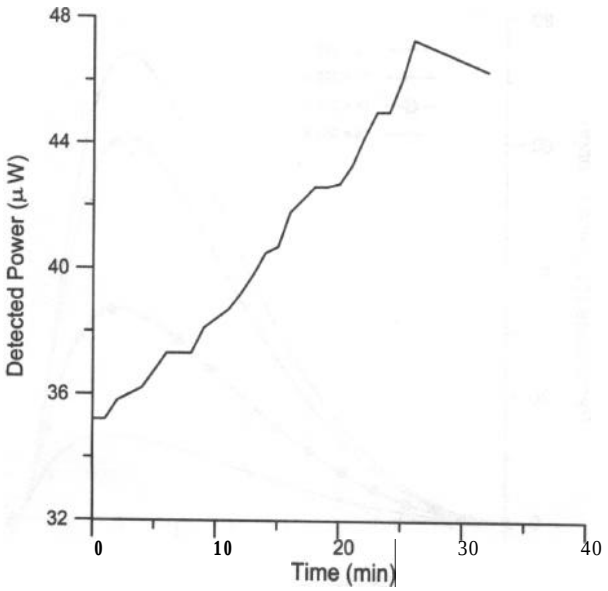

Fig. 5 Detected on-axis power versus time for an unpolarized target. The polarizer was being rotated in 1 0-deg increments once per minute for the first 26 min.

where T_{lo} is the initial temperature of the polarizer mount, T_{hi} is the increased mount temperature, R_{ave} is the average polarizer reflectivity [average of Eqs. (2a) and (2b)], and L_{ave} is as before. This model predicts that a temperature rise of 3.5 K will produce the 3% signal increase shown in Fig. 5 (measured after a thermal equalization period as discussed above).

5 Conclusion

We have explained three instrument effects that limit the quantitative interpretation of polarized infrared images. The first effect is image nonuniformity caused by narcissus. The second effect is partial polarization of off-axis image regions, caused by background radiance reflected into the camera by the wire-grid polarizer. We emphasize that the key to understanding the variation of detected radiance with polarizer angle is recognizing that the front and back surfaces of the polarizer act as a polarizer-analyzer pair. The third effect is frictional heating of the polarizer mount, which causes the mean detected radiance to increase with successive polarizer rotations. These instrument effects will have to be considered carefully to achieve the calibration uncertainties (on the order of 1%) required in several remote-sensing applications we are investigating.

Acknowledgment

This work was carried out at Dr. Eustace Dereniak's Optical Detection Laboratory of the Optical Sciences Center at The University of Arizona. J. H. Churnside of NOAA provided valuable suggestions, as did the reviewers.

References

1. D. Lemke, U. Grozinger, I. Heinrichsen, U. Klaas, P. Lutzow-Wentzky, J. Schubert. F. Garzon. W. Kratschmer, M. Wells. H.-P. Gemund, E. Kreysa, and J. Wolf, "Far-infrared imaging, polarimetry, and spectrophotometry on the Infrared Space Observatory," *Opt. Eng.* **33**(1), 20-25 (1994).
2. T. J. Rogue, F. G. Smith, and J. E. Rice, "Passive target detection using polarized components of infrared signatures," *Proc. SPIE* **1317, 242-**251 (1990).
3. R. D. Tooley, "Man-made target detection using infrared polarization," *Proc. SPIE* **1166, 52-58 (1989).**
4. J. H. Churnside, S. G. Hanson, and J. J. Wilson, "Determination of ocean wave spectra from images of backscattered incoherent light," *Appl. Opt.* **34**(6), 962-968 (1995).
5. Y. Takano and K. N. Liou, "Infrared polarization signatures from cirrus clouds." *Appl. Opt.* **31**(12), 1916-1919 (1992).
6. J. W. Howard and I. R. 'Abel, "Narcissus: reflections on retroreflections in thermal imaging systems," *Appl. Opt.* **21**(18), 3393-3397 (1982).
7. M. Born and E. F. Wolf, *Principles of Optics*, 6th ed., p. 42, Pergamon, Elmsford, NY (1980).

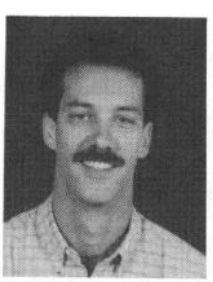

Joseph A. Shaw received a BS in electrical engineering from the University of Alaska/Fairbanks in 1987, a MS in electrical engineering from the University of Utah in 1989, and a MS in optical sciences from the University of Arizona in 1994. Currently he is a PhD candidate at the University of Arizona Optical Sciences Center. Mr. Shaw has been an electronics engineer at the Environmental Technology Laboratory (formerly the Wave Propagation Laboratory) of the National Oceanic and Atmospheric Administration in Boulder, Colorado, since 1989. His responsibility there is the development of optical, infrared, and millimeter-wave systems for atmospheric and oceanic remote sensing.

Michael R. Descour: Biography and photograph not available.